



## Resistivity structure of a seismic gap along the Atotsugawa Fault, Japan

Tada-nori Goto\*, Yasuo Wada, Naoto Oshiman, Norihiko Sumitomo<sup>1</sup>

*Disaster Prevention Research Institute, Kyoto University Gokasho, Uji, Kyoto 611-0011, Japan*

Received 14 April 2004; received in revised form 27 July 2004; accepted 4 August 2004

### Abstract

Seismicity along the Atotsugawa Fault, located in central Japan, shows a clear heterogeneity. The central segment of the fault with low-seismicity is recognized as a seismic gap, although a lot of micro-earthquakes occur along this fault. In order to elucidate the cause of the heterogeneity in seismicity, the electrical resistivity structure was investigated around the Atotsugawa Fault by using the magnetotelluric (MT) method. The regional geoelectrical strikes are approximately parallel to the fault in a low-frequency range. We constructed two-dimensional resistivity models across the fault using TM-mode MT responses to minimize three-dimensional effects on the modeling process. A smooth inversion algorithm was used, and the static-shifts on the apparent resistivity were corrected in the inversion process.

A shallow, low resistivity zone along the fault is found from the surface to a depth of 1–2 km in the best-fit model across the high-seismicity segment of the fault. On the other hand, the corresponding low resistivity zone along the low-seismicity segment is limited to a shallower depth less than 1 km. The low resistivity zone along the Atotsugawa Fault is possibly due to fluid in the fracture zone; the segment with higher levels of seismicity may have higher fluid content in the fault zone compared with the lower seismicity segment. On a view of the crustal structure, a lateral resistivity variation in a depth range of 3–12 km is found below the fault trace in the high-seismicity segment, while a resistive layer of wide extent is found at a depth of about 5 km below the fault trace in the low-seismicity segment. The resistive layer is explained by less fluid condition and possibly characterized as high rigidity. Differences in the resistivity structures between low and high-seismicity segments of the fault suggest that the seismic gap in the central part of the Atotsugawa Fault may be interpreted as a locked segment. Thus, MT is an effective method in evaluating a cause and future activity of seismic gaps along active faults.

The lower crust appears as a conductive zone beneath the low-seismicity segment, less conductive beneath the high-seismicity segment. Fluid is inferred as a preferable cause of the conductive zone in this study. It is suggested that the conductive lower

\* Corresponding author. Present address: Japan Agency for Marine-Earth Science and Technology, 2-15 Natsushima, Yokosuka 237-0061, Japan. Tel.: +81 46 867 9335; fax: +81 46 867 9315.

*E-mail address:* [tgoto@jamstec.go.jp](mailto:tgoto@jamstec.go.jp) (T.-n. Goto).

<sup>1</sup> Present address: Faculty of Humanities and Sciences, Kobe Gakuin University, 518 Arise, Ikawadani-cho, Nishi-ku, Kobe 651-2180, Japan.

crust beneath the low-seismicity segment is recognized where fluid is trapped by an impermeable layer in the upper crust. On the other hand, fluid in the lower crust may upwell to the surface along the high-seismicity segment of the fault.

© 2004 Elsevier B.V. All rights reserved.

**Keywords:** Seismic gap; Magnetotellurics; Atotsugawa Fault; Resistivity; Active fault

## 1. Introduction

Recent dense GPS network (GEONET) by the Geographical Survey Institute, Japan, has clearly shown a narrow deformation zone with a large convergence rate of 20 mm/year along the Niigata-Kobe Tectonic Zone (NKTZ in Fig. 1), which is supposed to be a plate boundary (Sagiya et al., 2000). In the NKTZ, a number of quaternary active faults are concentrated, and large

earthquakes have recently occurred. The Atotsugawa Fault with length of 60 km is one of the most active faults in the NKTZ (Research Group for Active Faults, 1991). Fig. 1 shows the location of the Atotsugawa Fault with a geological setting around the Atotsugawa region. The Atotsugawa Fault is a strike-slip fault with a right lateral displacement (Matsuda, 1966). The strike of the fault trace is approximately N60°E, and the fault plane is almost vertically ( $90^\circ \pm 10^\circ$ ) near the surface. From geological studies, activity of the Atotsugawa Fault started in the latest tertiary (Matsuda, 1966). There have been several large historical earthquakes along the Atotsugawa Fault; one of the largest events was the 1858 Ansei Hida earthquake with a magnitude of about 7.0 (summarized in Mikumo et al., 1988).

Seismicity along the Atotsugawa Fault is clearly recognized as a belt-like concentration of epicenters (Ito and Wada, 1999). The distribution of epicenters around the Atotsugawa region is shown in Fig. 2(a). A lineament of the epicenters is clearly recognized, corresponding to the surface trace of the Atotsugawa Fault. The focal depths along the fault are shallower than 15 km as shown in Fig. 2(b). In addition, a spatial heterogeneity of the seismicity along the Atotsugawa Fault is clearly recognized (Mikumo et al., 1988; Ito and Wada, 1999). The seismicity along the central segment (CAF) of the Atotsugawa Fault is rather low delineated by a dashed curve in Fig. 2(b) compared with the eastern (EAF) and western (WAF) segments of the fault. In other words, a seismic gap is recognized in the central segment of the Atotsugawa Fault.

There are several hypotheses for the seismic gap in the CAF. The Geographical Survey Institute, Japan (1997) observed baseline length across the Atotsugawa Fault and found a creep-like movement with the rate of about 1.5 mm/year in the CAF. They also reported no observable baseline change at another site near the western segment of the Atotsugawa Fault (WAF). Their geodetic observation suggests that the seismic gap may correspond to a large creep zone along the CAF. On the other hand, Mikumo et al. (1988) argued that the

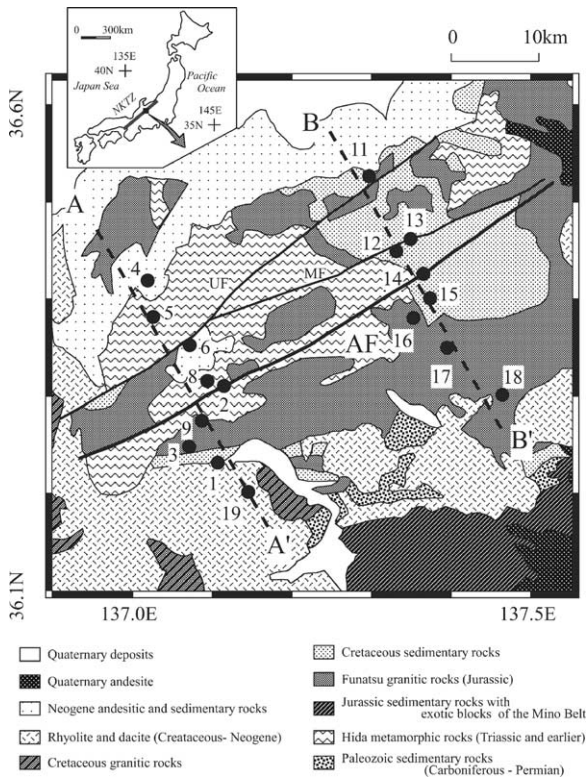


Fig. 1. Locations of MT sites (circles with site numbers) and a simplified geological map (Geological Survey of Japan, 1989). The Atotsugawa Fault is shown as a thick line (AF). Other major active faults (UF: the Ushikubi fault; MF: the Mozumi fault) are also shown. The Niigata-Kobe Tectonic Zone (Sagiya et al., 2000) is shown in the upper-left panel as a gray line.

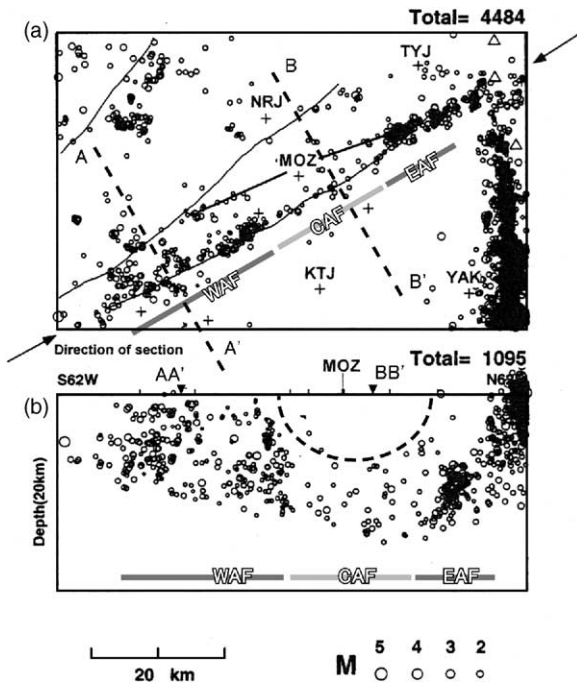


Fig. 2. Distribution of the earthquakes around the Atotsugawa region from 1996 to 1999 (redrawn from Ito and Wada, 1999): (a) epicenter distribution and (b) focal depth section along the Atotsugawa Fault denoted by arrows in (a). The western, central and eastern segments of the Atotsugawa Fault are denoted by WAF, CAF and EAF, respectively. A seismic gap at shallow depth in the CAF is indicated by a dashed line. Two MT profiles (AA' and BB') are also drawn.

heterogeneous seismicity along the Atotsugawa Fault may be related to postseismic stress concentration after the 1858 Hida earthquake resulted from the heterogeneity of the fault strength. Similar relationships between a main shock and aftershocks are well studied on large earthquakes along subducting plates. For example, Nagai et al. (2001) studied seismic records of two large earthquakes of magnitude greater than 7, which repeatedly occurred off the northeast coast of Japan in 1968 and 1994. They concluded that two earthquakes have a common rupture zone surrounded by their aftershocks, and interpreted the rupture zone as an asperity, as proposed by Lay et al. (1982). In an asperity, a rupture zone is locked during its preparation period so that it exhibits low-seismicity, but suddenly radiates a seismic wave with large magnitude. In the case of the Atotsugawa Fault, it is possible that the seismic gap in the CAF is due to a locked segment along the active fault. Recently, dense GPS surveys across the

CAF were carried out (Hirahara et al., 2003), and the observed horizontal displacements are approximately explained by a simple model with the locked Atotsugawa Fault from the surface to a depth of 15 km and a strain rate of 20 mm/year in an EW direction. However, observed displacements near the Atotsugawa Fault do not agree with predicted ones from this model, and possibility of a fault creep at the CAF cannot be excluded.

In order to elucidate the reason of heterogeneity in seismicity along the Atotsugawa Fault, the resistivity structure in the Atotsugawa region has been investigated in this study. As shown in previous studies (e.g., Electromagnetic Research Group for the Active Fault, 1982; Handa and Sumitomo, 1985; Jones et al., 1992; Unsworth et al., 1997, 1999, 2000), low resistivity zones have been often found along active faults. Such low resistivity zones are interpreted to be caused by fluid in fracture zones (e.g., Unsworth et al., 1997) and/or conductive carbon concentrated by upwelling of water in fracture zones (e.g., Jones et al., 1992). Therefore, the scale of a low resistivity zone along a fault can be used as an index of fault activities. In this study, the magnetotelluric (MT) sounding and the geomagnetic depth sounding (GDS) methods were carried out along two profiles across the Atotsugawa Fault as shown in Fig. 1.

## 2. Observation

Two profiles of the MT soundings were chosen around the Atotsugawa region, as shown in Figs. 1 and 2. Profile AA' is located across the high-seismicity segment along the Atotsugawa Fault (WAF), while profile BB' is over the low-seismicity segment (CAF). Sites 2 and 14 were located on the fracture zone of the Atotsugawa Fault. Natural fluctuations in the electric and the magnetic fields were observed around the Atotsugawa region in 1994 and 1995. Two MT instruments (V5 systems by Phoenix Geophysics Ltd., Canada), covering a wide frequency band from 400 to 0.0005 Hz, were used simultaneously with synchronized clocks. Induction coils were used as magnetic sensors, and electrodes of Pb–PbCl<sub>2</sub> type with separations of 30–100 m were used for measuring horizontal electric fields. Three magnetic and two electric components were recorded over 3–4 days at each site. A combination of fast Fourier transforms and cascade

decimation technique (Wight and Bostick, 1980) was used for obtaining the auto and cross power spectra. The total numbers of stacked power spectra were about 20,000 around 1 Hz and about 100 around 0.01 Hz.

Simultaneous time series data with two instruments, separated by a distance of 20 km at least, were obtained and the remote reference processing (Gamble et al., 1979) was applied to estimate impedance tensors. In 1995, another remote reference site was set up at the part of northern Kyoto Prefecture, 250 km west from the Atotsugawa region. The impedance tensors obtained by using this far-remote site were nearly same as ones obtained by using a local remote reference site in the Atotsugawa region. Therefore, the separation distance of 20 km is large enough for the stable estimation of impedance tensors in this study. Most of obtain apparent resistivities and impedance phases, called as MT responses, showed small errors and high multiple-coherencies between the electric and magnetic fields. However, large cultural noise at Sites 1, 3, 16 and geomagnetic quiescence during observation at Sites 9 and 12 result in low-quality MT responses with large errors and the low multiple-coherencies. In this study, low-quality MT responses with large phase errors ( $>30^\circ$ ) are limited at several sites and frequencies, and showed less smooth changes to frequency variations. Therefore, the observed impedance with phase errors greater than  $30^\circ$  were rejected in the following analyses and modeling. The remaining impedances exhibit high multiple-coherences ( $>0.8$ ).

### 3. Strike direction and induction arrow

The strike directions were calculated with the method of Chakridi et al. (1992). This method avoids the effect of surficial galvanic distortion (Groom and Bailey, 1989). The impedance tensor can be rotated, and if the rotation angle corresponds with the regional geoelectrical strike, then the following equations

$$\begin{aligned} \arctan \left( \frac{\text{imag}(Z_{xx}/Z_{yx})}{\text{real}(Z_{xx}/Z_{yx})} \right) &= 0, \\ \arctan \left( \frac{\text{imag}(Z_{xy}/Z_{yy})}{\text{real}(Z_{xy}/Z_{yy})} \right) &= 0 \end{aligned} \quad (1)$$

are satisfied, where  $Z_{xx}$ ,  $Z_{xy}$ ,  $Z_{yx}$  and  $Z_{yy}$  are elements of a rotated impedance tensor at a frequency. In this study, a similar method by Jones and Groom (1993:

Eqs. (10) and (11)) is also used because the Chakridi's method is not effective in a case of no distortion. On the Jones and Groom's method, the following equations are satisfied when an angle between the rotated direction and the regional strike is  $45^\circ$

$$\begin{aligned} \arctan \left( \frac{\text{imag}((Z_{xx} + Z_{xy})/(Z_{yx} + Z_{yy}))}{\text{real}((Z_{xx} + Z_{xy})/(Z_{yx} + Z_{yy}))} \right) &= 0, \\ \arctan \left( \frac{\text{imag}((Z_{xx} - Z_{xy})/(Z_{yx} - Z_{yy}))}{\text{real}((Z_{xx} - Z_{xy})/(Z_{yx} - Z_{yy}))} \right) &= 0 \end{aligned} \quad (2)$$

We rotated an observed impedance tensor at a site every  $2^\circ$  and searched a rotation angle to satisfy Eq. (1). A standard deviation of rotated angles from Eq. (1) in a frequency range of 300–0.001 Hz is also estimated at each site. Similarly, rotation angles and a standard deviation are calculated from Eq. (2). Finally, the method by Eqs. (1) and (2) giving the smaller standard deviation is chosen at each site as the better method for strike estimation.

The distribution of the regional strike averaged over the frequency range of 100–0.001 Hz at each site (solid line) is shown in Fig. 3(a). We note that the regional strike is approximately parallel (or perpendicular) to the Atotsugawa Fault. Real induction vectors (Parkinson vectors) over a frequency range of 1–0.1 Hz are shown as arrows in Fig. 3(a), approximately perpendicular to both the regional strike and the Atotsugawa Fault. Histograms of the strike in four respective frequency bands along each profile are shown in Fig. 3(b). Although a slightly large dispersion of the strike direction is seen in the frequency range of 10–1 Hz, the strike directions are stable at the frequency range lower than 1 Hz. The averaged strike directions at 1–0.01 Hz along AA' and BB' are N80°E and N45°E, respectively. Thus, the regional structure around the Atotsugawa region is approximately two-dimensional with a NE or ENE strike, while the shallow structure has a three-dimensional character.

### 4. Apparent resistivity and phase

The pseudosections of the observed apparent resistivity and the impedance phase along the profiles AA' and BB' are shown in Fig. 4(a) and (b), respectively. Here, N30°W was taken as the  $x$ -axis of the coordinate and N60°E as the  $y$ -axis, respectively. The curves of

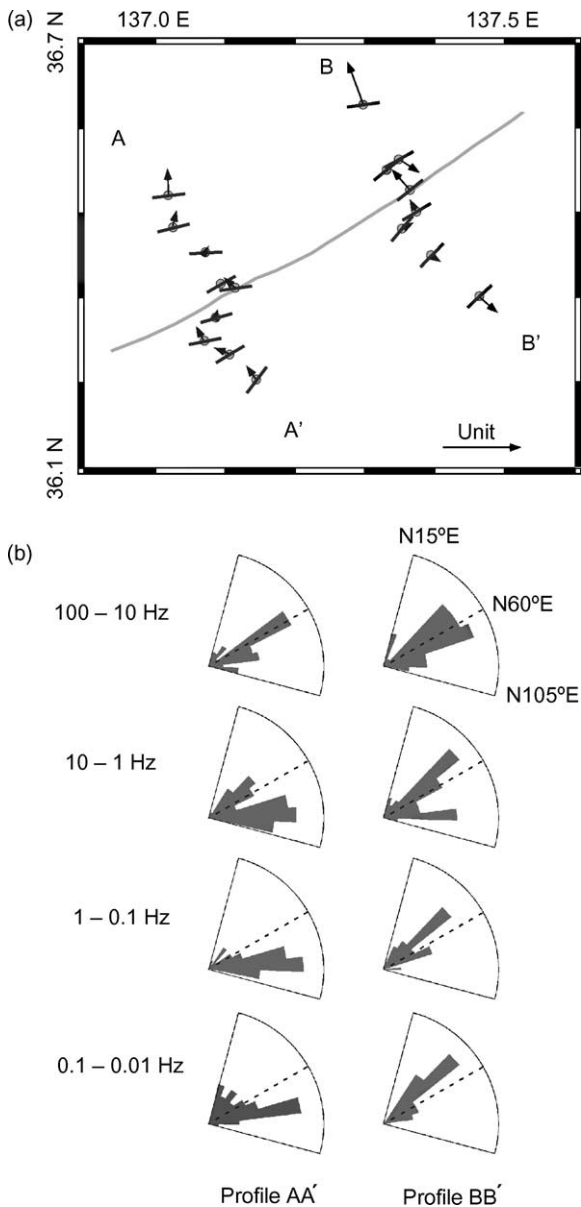


Fig. 3. (a) Distribution of the regional strike averaged in a frequency of 100–0.001 Hz at each site. Real induction vectors (Parkinson vectors) averaged in a frequency of 1–0.1 Hz are also shown with a unit vector. (b) Histograms of the regional strikes in four frequency bands along the profiles AA' and BB'. The regional strikes from N15°E to N105°E are used for these plots. The strike of the Atotsugawa Fault, N60°E, is also shown as dashed lines.

both the apparent resistivity and phase are shown in Fig. 7, in which standard errors of the MT response are also plotted.

Along the profile AA', the apparent resistivity and phase change sharply near the Atotsugawa Fault (Site 2). At Sites 4, 5 and 8 located in the northern side of the fault, larger values of the apparent resistivity ( $\rho_{xy}$  and  $\rho_{yx}$ ) are apparent in the lower frequency range. On the other hand, the apparent resistivity decreases toward the lower frequency range in the southern side of the fault (Sites 9, 3, 1, and 19). Moreover, the phase values ( $\varphi_{xy}$  and  $\varphi_{yx}$ ) in the northern sites of the fault are also smaller than 45° at the frequency range higher than 1 Hz, while they are larger than 45° in the southern sites. These observed features imply that an underlying layer is resistive in the northern area of the WAF, while it is conductive in the southern area of the WAF. It is suggested, therefore, that the WAF possibly corresponds to a lateral resistivity boundary. Note MT responses at Site 6 where the apparent resistivity is much lower than ones at Sites 5 and 8, but the phase values at the three sites are similar. Such low apparent resistivities at Site 6 could be interpreted as a negative static-shift as described by Jones (1992: see Figs. 3–5 in his paper).

By contrast, the apparent resistivity and phase along the profile BB' gradually change across the fault, as shown in Fig. 4(b). The apparent resistivity increases with its maximum at about 5 Hz, with the lower apparent resistivity at the lower frequency. Also, the phase value becomes low at 10 Hz and high at 0.1 Hz along the profile BB'. These features suggest that a resistive layer widely spreads and a deep conductive layer underlies beneath the profile BB'.

## 5. Two-dimensional modeling with static-shift correction

In the Atotsugawa region, resistivity models were constructed to explain the observed MT response along each profile. As described above, the resistivity structure is thought to be approximately two-dimensional (2D) with the strike parallel to the Atotsugawa Fault (N60°E), while the shallow structure is three-dimensional (3D). Wannamaker et al. (1984) showed that 2D modeling routines of the transverse electric (TE) mode applied to MT responses on a 3D conductive body near the surface can make false low

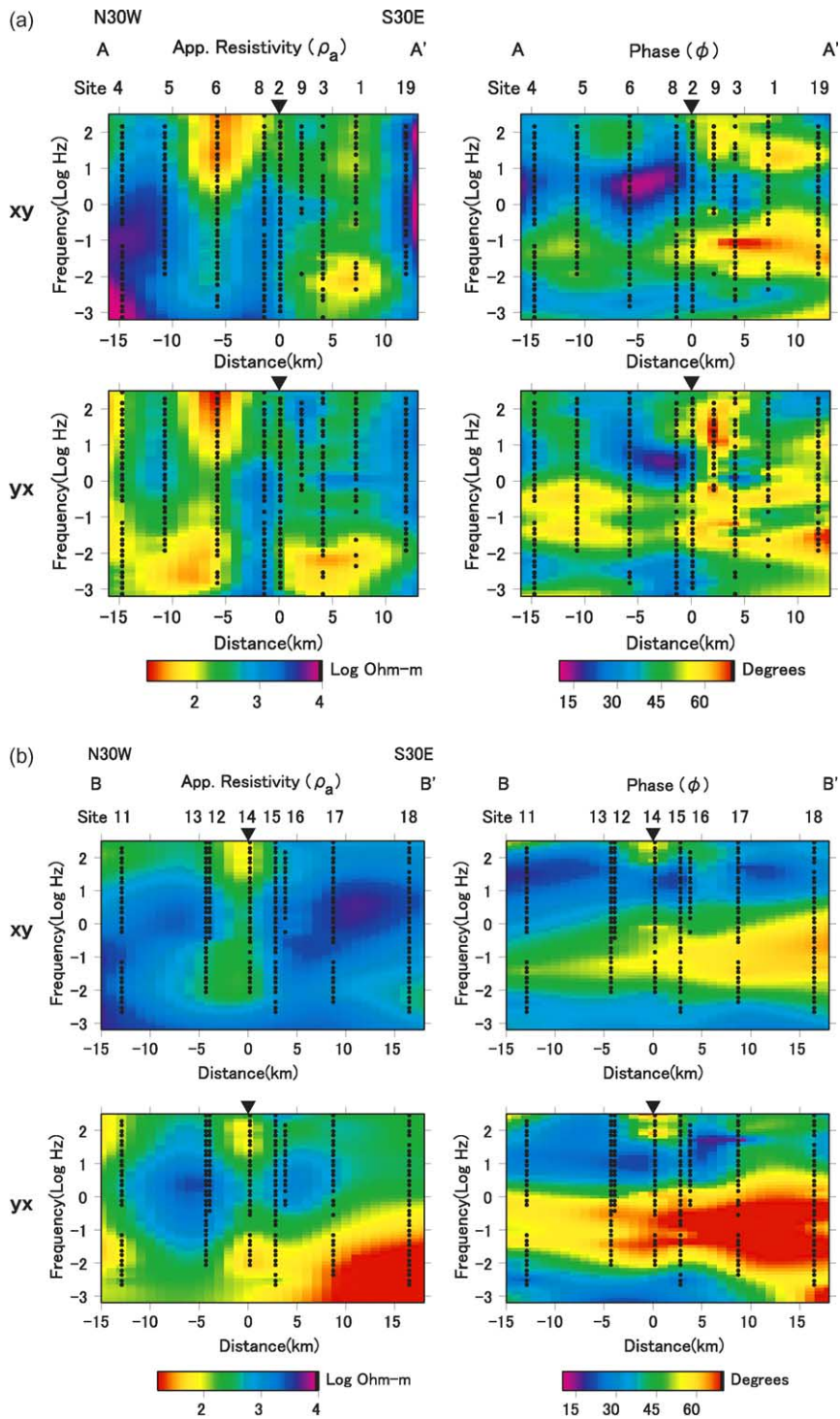


Fig. 4. Pseudosections of observed apparent resistivity and impedance phase along (a) the profile AA', and (b) the profile BB'. Observed data points used for pseudosections are plotted as small circles. Inverted triangles indicate the surface location of the Atotsugawa Fault.

resistivities at depth. This is because the TE modeling algorithm do not account for the effects of charges at resistivity boundaries. They also showed that the elongated 3D body may be modeled accurately with a 2D modeling of the transverse magnetic (TM) mode on centrally located profiles across the 3D body. This is because the TM modeling algorithm includes boundary charges in its formulation. Therefore, we used only the apparent resistivity and phase in the TM-mode ( $\rho_{xy}$  and  $\varphi_{xy}$ ) for modeling in order to minimize 3D effects in the 2D modeling.

Static effects or static-shifts, recognized as DC-shifts on logarithmic apparent resistivity (e.g., Jones,

1992), should be removed because an erroneous resistivity structure is obtained by inversion procedures. An observed electric field ( $E_o$ ) at the surface is expressed by regional electric field ( $E_p$ ) and local electric field generated by the surface heterogeneity ( $E_s$ ) as follows:

$$E_o = E_p + E_s \tag{3}$$

The static-shift is due to  $E_s$  field generated by a charge buildup at a near-surface resistivity boundary (Ogawa, 1992). Such effects of the surface heterogeneity to the static-shift can be confirmed by forward MT responses with 2D resistivity models (Fig. 5(a) and (b)). The model in Fig. 5(b) is based on Fig. 5(a) but anoma-

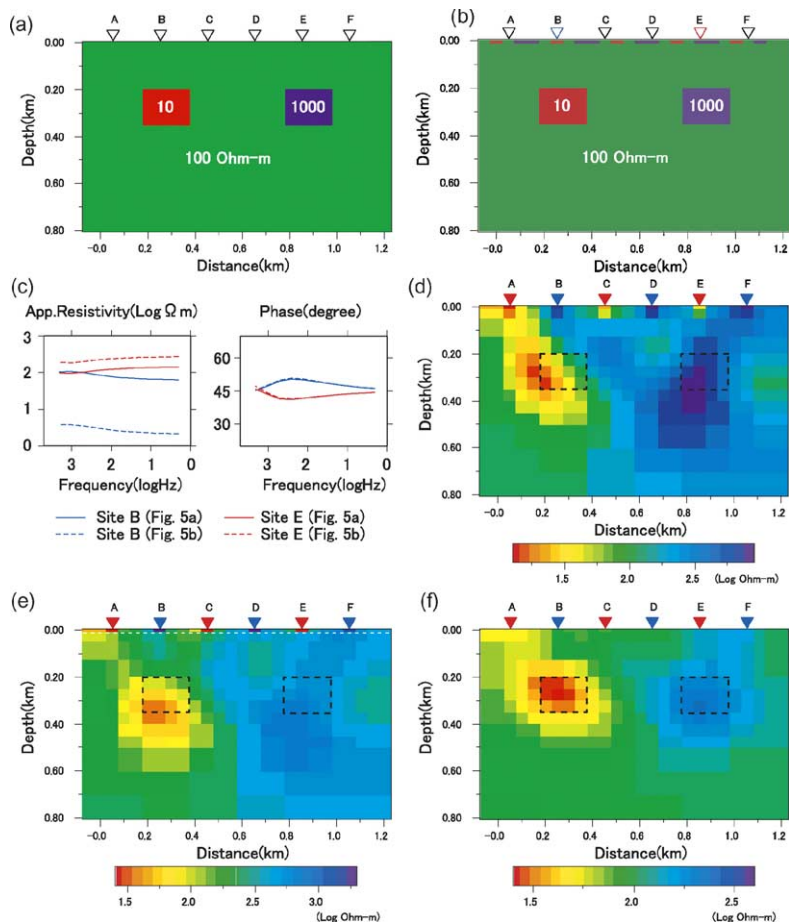


Fig. 5. (a) Resistivity model for a synthetic MT response. MT sites are indicated by inverted triangles. (b) Same as (a) but resistivity blocks of 10 and 1000 Ωm are inserted into the surface layer. (c) TM-mode apparent resistivity and phase curves at Sites B and E calculated from the models in (a) and (b). (d) Model obtained by ordinary inversion but distorted by static-shifts. (e) Model obtained by our inversion procedure with a highly heterogeneous surface layer. A white broken line indicates the bottom of surface layer. (f) Final model obtained after the static-shift correction. See the main text for details.

lous blocks with thickness of 10 m and resistivity of 10 and 1000  $\Omega\text{m}$  are inserted into the surface layer. We used a program by Uchida and Ogawa (1993) to calculate forward MT responses. Comparing MT responses from these models, shown in Fig. 5(c), DC level of the TM apparent resistivity curve is affected by anomalous surface blocks, but the TM phase indicates little effects.

Unexpected effects of static-shifts in modeling procedure are demonstrated by a smooth inversion algorithm. Apparent resistivity and phase values in the TM-mode are calculated in a frequency range of 2–2050 Hz on a 2D model shown in Fig. 5(a). Then, static-shifts are added to the calculated apparent resistivity: positive shifts to Sites A, C and E with factor of 10 and negative shifts to Sites B, D and F with factor of 0.1, respectively. When such DC-shifted MT responses are used with an ordinary 2D inversion by Uchida and Ogawa (1993), the obtained model is shown in Fig. 5(d). Although resistive and conductive zones are imaged in the model, those locations are incorrect, and the shallow structure is strongly distorted by the static-shift. The inversion algorithm by Uchida and Ogawa (1993) and deGroot-Hedlin and Constable (1990) and so on are based on the smooth resistivity model. Unacceptable inversion result as shown in Fig. 5(d) is possibly due to difficulty on imaging high heterogeneity of the near-surface resistivity by using a smooth model.

We propose a new simple method for the static-shift correction by using a 2D inversion with smoothness constraints based on Uchida and Ogawa (1993). As shown in Fig. 5(c), the surface heterogeneity can show the static effect in the TM apparent resistivity. Therefore, a highly heterogeneous surface layer with thickness of 10 m, appended on a 2D smooth resistivity model, is used to express static-shifts in the model. The detailed correction process is summarized as follows. First, the 2D inversion with a heterogeneous surface layer overlying a smooth block structure is carried out using the observed TM responses. In order to make the surface layer heterogeneous, the weighting for the smoothness calculation (see Eq. (A.2) in Uchida, 1993) was modified at the surface blocks beneath MT sites as follows: (i)  $c_{14} = 0$  between the surface and underlying block; (ii)  $c_{12} = c_{13} = 0.1D/(2(W + D))$  between the surface and neighboring blocks. Other blocks have ordinary weights as in Uchida (1993). This weighting means that high resistivity contrast can be allowed only between the surface blocks beneath MT sites and the

surrounding blocks. Although all of the weighting at the surface should be zero to make the surface blocks less smooth to the surrounding blocks, such ideal weighting yields extremely high or low resistivity values in the surface blocks and makes the forward and inversion calculations unstable (with overflow or underflow). Therefore, we practically selected the weighting with the above value for  $c_{12}$  and  $c_{13}$  as small as possible, based on a number of synthetic tests such as described later.

In order to estimate static-shift factors, two synthetic TM-mode responses at MT sites are estimated after the first inversion was done: MT responses from the best-fit model and from the same model but resistivity in the surface layer (a part of model shallower than a white broken line in Fig. 5(e)) are replaced by the underlying blocks. In other words, two MT responses with and without the highly heterogeneous surface layer are obtained. In most cases, these two apparent resistivity curves have a similar shape but a different DC level, and the phases coincide within  $5^\circ$  such as shown in Fig. 5(c). Therefore, we adopt a mean difference between two apparent resistivity curves as a static-shift factor at each site. In order to avoid the upward or downward bias of the estimated static-shifts, the obtained factors are shifted as an average value of the factors from all sites is zero. Finally, observed MT responses, in which the static-shifts were corrected, are used for the ordinary inversion without the weighting for heterogeneous surface. Our correction method has a similar concept of deGroot-Hedlin (1991) and Ogawa and Uchida (1996) that the static-shifts are corrected in inversion procedures. A benefit in our method is to deal with surface heterogeneity directly in the resistivity model. For example, known information of the surface resistivity can be inserted into a highly heterogeneous layer in our inversion to estimate the static-shift factors more accurately.

The synthetic MT responses yielding the model in Fig. 5(d) are used again for testing the effectiveness of our static-shift correction. The thickness of the surface block was set as 10 m. A uniform earth of 100  $\Omega\text{m}$  is selected as an initial model. The model obtained by a ‘first’ inversion with the highly heterogeneous surface is shown in Fig. 5(e). The extremely high and low resistivity blocks in the surface layer are responsive to the assumed static-shifts. The final model obtained after the static-shift correction is shown in Fig. 5(f). Both conductive and resistive prisms are imaged on

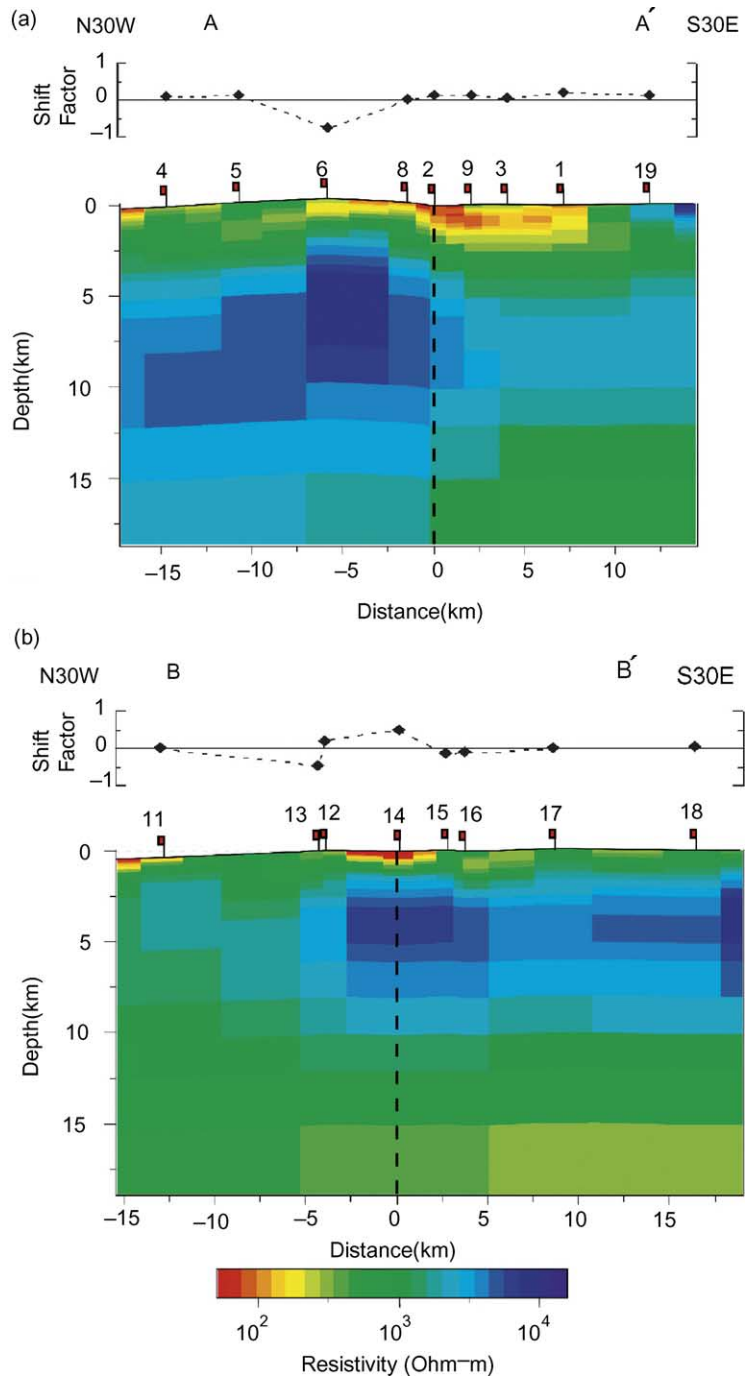


Fig. 6. Two-dimensional resistivity models along (a) the profile AA', and (b) the profile BB'. Flags indicate the locations of our MT sites. The location of the Atotsugawa Fault is indicated by a broken line. Logarithmic static-shifts factors estimated in this study are also shown.

the proper positions. In this case, any initial models result in similar final solutions as shown in Fig. 5(f). It is concluded that static-shifts in MT response are expressed by a highly heterogeneous surface with the above weighting, and can be effectively corrected by our method.

The 2D inversion with the static-shift correction was applied to the observed TM-mode MT responses around the Atotsugawa Fault (shown in Fig. 7). A strike of N60°E is chosen for the 2D modeling along profiles AA' and BB'. The width of the 2D model is taken

as 1500 km and the bottom depth is taken down to 2100 km. The number of elements is 55 in horizontal and 35 in vertical. The minimum element width of 0.9 km is assigned near the Atotsugawa Fault and the minimum thickness of 10 m is applied for a thin surface layer. A uniform earth of 1000  $\Omega\text{m}$  is used as an initial model for the inversion. A sufficient fitting between observed and calculated responses is achieved within 10 iterations.

The best-fit model along the profile AA' is shown in Fig. 6(a) with estimated static-shift factors; calcu-

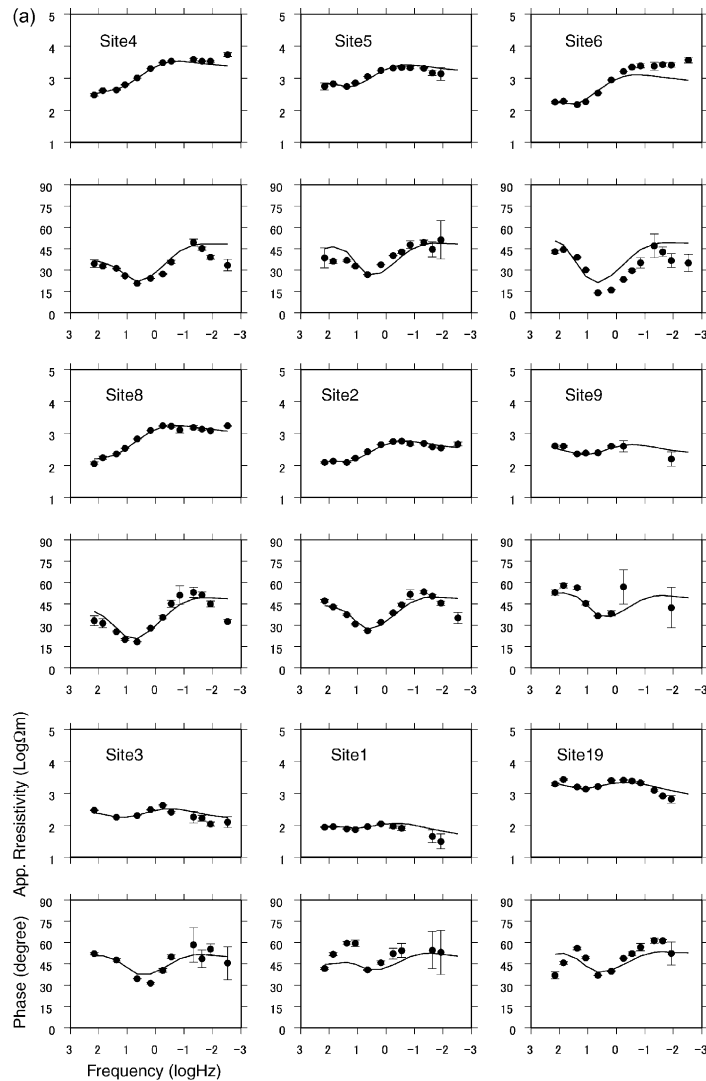


Fig. 7. Calculated apparent resistivity and impedance phases (lines) from the best-fit models in Fig. 6 along (a) the profile AA' and (b) the profile BB', respectively. The observed responses used for the inversion (circles) are shown together. Error bars of  $1\sigma$  are added.

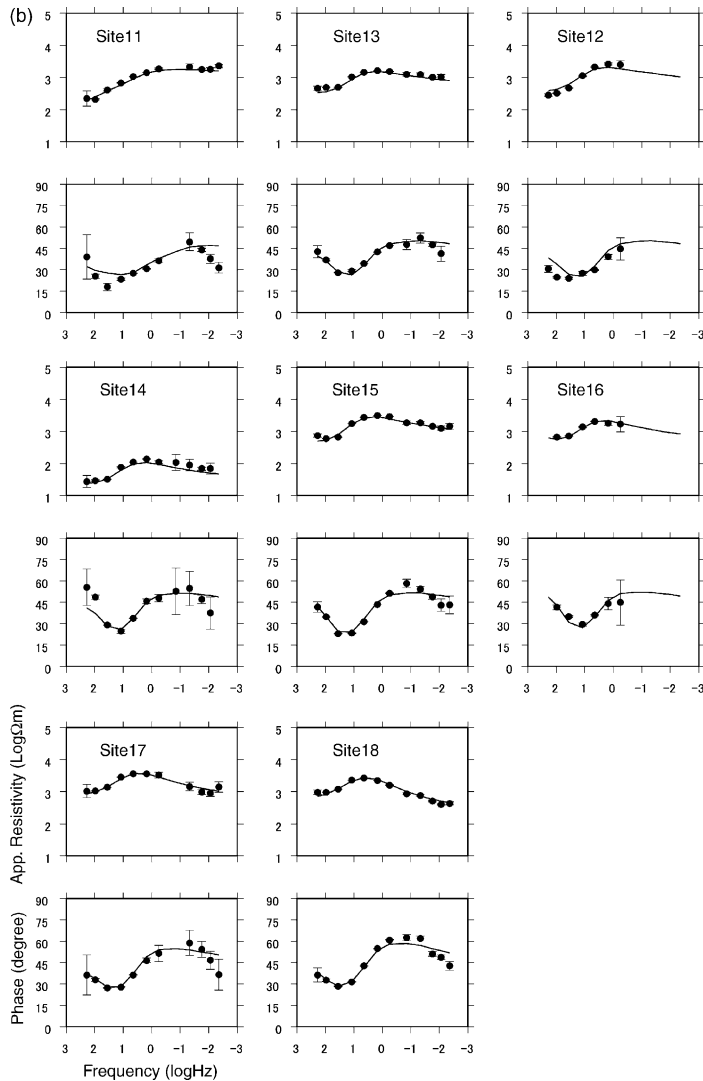


Fig. 7. (Continued).

lated apparent resistivity and phase from the best-fit model are shown in Fig. 7(a). The most remarkable and well-resolved feature in the model is a highly resistive zone ( $>4000 \Omega\text{m}$ ) below the northern area of the Atotsugawa Fault, and a moderately resistive zone in the southern area. This resistivity contrast near the fault well explains the observed features along the profile AA' that the apparent resistivity increases in the frequency range of 10–0.1 Hz at northern sites of the fault while it decreases at southern sites. Resistivity in the model decreases below a depth of 12 km, which

explains the observed high phase at the frequency of 0.05 Hz. The minimum resistivity value of the conductive layer is about  $600 \Omega\text{m}$  in depths of 12–20 km. At shallow depths, a low resistivity zone ( $<100 \Omega\text{m}$ ) is found along the WAF, extending to a depth of 1.4 km, with a minimum low resistivity of  $60 \Omega\text{m}$  beneath Site 2. These features are summarized in Fig. 8(a). Note that the estimated static-shift factor at Site 6 is a large negative value as predicted above.

The best-fit resistivity model for the profile BB' is shown in Fig. 6(b). Comparisons between the cal-

culated and observed MT responses were shown in Fig. 7(b). One of the major features in the model shown in Fig. 6(b) is a resistive layer ( $>4000 \Omega\text{m}$ ) of wide extent at a depth of about 5 km. The highest resistivity value of about  $7000 \Omega\text{m}$  is obtained just beneath the surface trace of the Atotsugawa Fault. This resistive layer is necessary to explain the low phase at 10 Hz observed at all sites along the profile BB'. Another feature in the best-fit model is a conductive layer ( $<800 \Omega\text{m}$ ) below a depth of about 12 km. The minimum resistivity value of the conductive layer is about  $300 \Omega\text{m}$  in depths

of 12–20 km. The deep conductive layer explains the observed high phase at 0.1 Hz and the apparent resistivity decreasing at the frequency less than 1 Hz. Finally, at shallow depths, a low resistivity zone ( $<100 \Omega\text{m}$ ) is found beneath Site 14, although its bottom is located at a depth of 0.4 km. The minimum value in the low resistivity zone is  $30 \Omega\text{m}$ . These features are summarized in Fig. 8(b).

Sensitivity of the best-fit model was checked using forward modeling. First, we checked sensitivity of a deep extension of the low resistivity zone along

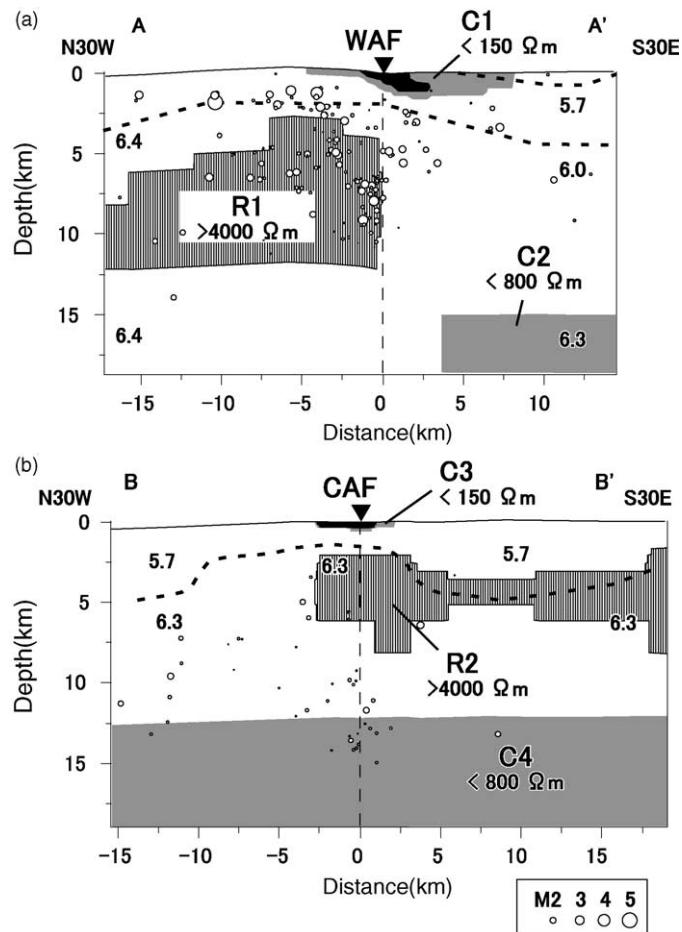


Fig. 8. Schematic diagram of the obtained resistivity structures (a) across the western segment and (b) the central segment of the Atotsugawa Fault. Surface traces of the Atotsugawa Fault are shown as inverted triangles. Major conductive and resistive zones in Fig. 6 are denoted by C1–C4 and R1–R2, respectively. Within the low resistive zones along the fault shown as gray (C1 and C3), extremely low resistive zones ( $<100 \Omega\text{m}$ ) are colored black. P-wave velocity structures from Iidaka et al. (2003) and Shimada (1996, pers. comm.) are overlaid by dashed lines with estimated velocity values. Hypocenters based on Ito and Wada (1999), which occurred in a horizontal width of 15 km along each profile, are plotted by circles.

the fault (C1 and C3 in Fig. 8). A low resistivity zone along the Atotsugawa Fault is inserted into the best-fit model along each profile (Fig. 6(a) and (b)) as shown in Fig. 9. The width and resistivity are assumed to be 2.5 km and 100  $\Omega\text{m}$ , respectively, based on the best-fit model along the profile AA' (Fig. 6(a)). The bottom depth of the low resistivity zone ( $D$  in Fig. 9) is varied from 1 to 12 km. The calculated TM-mode apparent resistivity curves at Sites 2, 9, 14 and 15 are shown in Fig. 9. At other sites, no major differences were found in calculated MT responses with various bottom depths ( $D$ ). At Sites 2 and 14, immediately in the fault zone, the difference between calculated and observed apparent resistivity values becomes larger as the bottom of the low resistivity zone becomes deeper. The only exception is the calculated response curve at Site 2 with the bottom depth of 1 km, which is almost same as one from the best-fit model. Therefore, it is concluded that the bottom depths of the low resistivity zone is inferred as 1–2 km along the WAF (C1), and less than 1 km along the CAF (C3), respectively. Comparison between

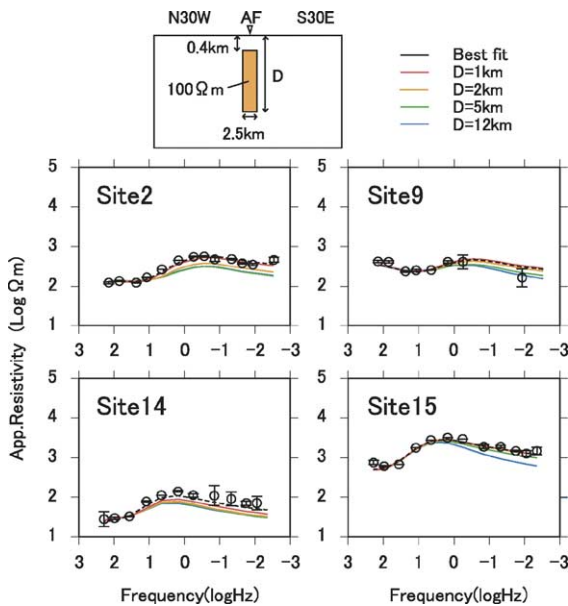


Fig. 9. Sensitivity tests on a depth extent of the low resistivity zone along the fault by forward modeling. Schematic view of the low resistive fault zone is shown in this figure (upper). Calculated MT responses at Sites 2, 9, 14 and 15 are shown (lower). Broken lines are calculated from the best-fit model in Fig. 6. Colored lines correspond to MT responses in cases of bottom depth ( $D$ ) of 1, 2, 5 and 12 km, respectively.

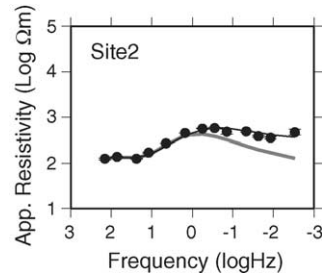


Fig. 10. Sensitivity test on the lower crust below the WAF by forward modeling. A solid line denotes a calculated MT response at Sites 2 from the best-fit model in Fig. 6(a). A gray line denotes a calculated MT response from the similar model with a conductive lower crust. See the main text for details.

the observed and calculated apparent resistivity values at Site 15 also supports that the low resistivity zone (C3) has no deeper extension than 5 km. Although the calculated MT response at Site 9 is affected by the low resistivity zone, the observed values show relatively large errors and cannot be used for the sensitivity test. Secondary, we checked whether the lower crust below the WAF is significantly less conductive than below the CAF or not. In this forward modeling, the resistivity values below the depth of 12 km along the profile BB' (Fig. 6(b)) are imposed to the corresponding parts of the best-fit model along the profile AA' (Fig. 6(a)). The calculated TM-mode apparent resistivity at Site 2 is denoted by a gray line in Fig. 10. A misfit between the synthetic and observed apparent resistivity is obvious. Therefore, it is concluded that a high conductive lower crust as shown below the CAF (C4 in Fig. 8) is not suitable below the WAF.

## 6. Discussion

### 6.1. Resistivity structure below the Atotsugawa Fault

The lateral variation of the resistivity structure below the WAF (with the northern highly and southern moderately resistive zones) is found at depths of 3–12 km by our magnetotelluric survey, which is a common feature in other geophysical surveys. A seismic experiment with explosive sources was conducted in the central Japan region (Iidaka et al., 2003), and a large lateral variation of P-wave velocity was found near the WAF as shown in Fig. 8(a). A magnetic survey near the profile AA' indicates that the total mag-

netic field in the north of the WAF is higher than in the south (Murakami et al., 1984). These geophysical surveys around the WAF imply the existence of lateral variation of the crustal structure below the WAF. On the other hand, the resistive block (R2 in Fig. 8) is found at the both side of the CAF. A similar P-wave velocity structure across the CAF was obtained by a 3D seismic tomography around the Atotsugawa Fault (Shimada, 1996, pers. comm.). The seismic velocity structure beneath the profile BB' were also shown in Fig. 8(b). The high resistivity layer at a depth of 5 km below the profile BB' approximately corresponds to the high velocity zone, and suggests that crustal structure is almost continuous across the CAF.

The shallow, low resistivity zones beneath Sites 2 and 14 (C1 and C3 in Fig. 8), immediately at the surface trace of the Atotsugawa Fault, are explained by a fracture zone along the fault. Low resistivity zones along active faults have often been found, and are probably related to fluid in the fracture zones. The existence of fluid in the fracture zone along the Atotsugawa Fault is supported by geochemical and self-potential measurements. Sugisaki et al. (1983) found a high concentration of H<sub>2</sub> in a fracture zone along the Atotsugawa Fault, and concluded that such concentration can be generated from a reaction between groundwater and fresh mineral surface formed by tectonic stresses in the fracture zone. Ohshiman et al. (1987) found a self-potential anomaly near the Atotsugawa Fault and concluded that groundwater flow in the fault plane generates this anomaly. Therefore, it is concluded that the shallow low resistivity zone near the Atotsugawa Fault is due to fluid in the fracture zone. As described above, the low resistivity zone along the WAF has a deeper extension than one along the CAF. If fluid has a similar resistivity along the Atotsugawa Fault, this difference of the low resistivity zone is caused by different porosity or pore connectivity between the WAF and the CAF on the basis of the Archie's law (Archie, 1942). In other words, the fracture zone in the shallow depth less than 2 km along the WAF has higher concentration or connectivity of fluid than one along the CAF.

### 6.2. Resistivity structure and seismic activity along the fault

Resistivity structures across the San Andreas Fault (SAF) are similar to our resistivity model, and give us

an interpretation of the seismic gap recognized in the CAF. Unsworth et al. (1997) conclude that the creep segment of the SAF at Parkfield is characterized by an extremely low resistivity zone, suggesting a high fluid concentration. However, Unsworth et al. (1999) found a narrow low resistivity zone along the SAF at Carrizo Plain, an apparently locked segment, with smaller conductance than at Parkfield. Therefore, the low resistivity zone along the CAF (C3), with shallower bottom than along the WAF (C1), is compared not to the extremely low resistivity zone along the creep segment of the SAF, but to the narrow low resistivity zone along the locked segment of the SAF. In addition, resistive blocks are present on the both side of the locked segment of the SAF (Mackie et al., 1997; Unsworth et al., 1999), which is similar to the resistivity structure across the CAF (R2). Meanwhile, a resistive block is imaged west of the fault at the creep segment of the SAF, while a conductive block is required to the east (Unsworth et al., 1997), which is similar to the structure across the WAF. These similarities on the resistivity structures inside and outside of the fault zones between the Atotsugawa Fault and the SAF support that the seismic gap at the CAF is interpreted not as a creep segments, but as a locked segment.

Our resistivity structures of the upper crust (in a depth range of 3–12 km) also indicate that the CAF has a character of main rupture zones of large earthquakes. In this study, the high resistive layer across the CAF (R2) is interpreted as a low porosity zone and possibly has high rigidity, and little micro-earthquake occurs within it. On the basis of the seismic studies, the main rupture zones are mostly limited to high velocity (i.e., high rigidity) regions as reported by Zhao and Kanamori (1995) and Chiarabba and Amato (1997). Eberhart-Phillips et al. (1990) found a high velocity and high resistivity zone corresponding to a main rupture zone of the Loma Prieta earthquake. A theoretical study on faulting in inhomogeneous media (Rybicki and Yamashita, 2002) supports the correlation between a main rupture zone and a high rigidity zone. These geophysical studies imply that the CAF across the high resistivity layer can be an asperity.

Our interpretation that the CAF is possibly a locked segment is supported by a frequency-magnitude relationship of micro-earthquakes at the CAF, characterized using the *b*-value. The *b*-value is a constant defined as the following equation (Gutenberg and Richter,

1944):

$$\log N(M) = A - bM$$

where  $A$  is a constant and  $N$  is a number of earthquakes in an area with magnitude greater than  $M$ . Mikumo et al. (1988) analyzed earthquakes occurred in 1977–1986 along the Atotsugawa Fault, and reported that the  $b$ -values are 0.81 for the WAF and 0.50 for the CAF, respectively. Amelung and King (1997) found that  $b$ -value in a creep segment along the SAF is greater than the neighboring segments. Hirose et al. (2002) also found several areas with anomalously high  $b$ -values in the northeastern Japan subduction zone, and no asperities correspond to the high  $b$ -value areas. These studies support that the seismic gap along the CAF is interpreted as a locked segment rather than a creep segment.

Similar resistivity structures to the CAF (Fig. 6(b)) have been reported along other faults except for the SAF. In central Japan, Kasaya et al. (2002) carried out a magnetotelluric survey around an earthquake fault of the 1984 Western Nagano Prefecture earthquake ( $M_{\text{w}}$  6.8), and compared the resistivity structure with seismic activity in 1995, about 10 years after the earthquake. They concluded that a recent low-seismicity region along the earthquake fault shows a reasonably homogeneous crust, corresponding to the CAF. Meanwhile, they concluded that a recent high-seismicity region with micro-earthquakes along the fault is characterized by a lateral resistivity variation, similar to the WAF. In Turkey, resistivity structures around a rupture zone of the 1999 Izmit earthquake ( $M_{\text{w}}$  7.4), which had been known as a seismic gap along the North Anatolian fault zone until this earthquake, were obtained immediately after the earthquake. The results indicate that the main shocks are located at northern edge of a high resistive zone (Oshiman et al., 2002) and after-shocks along the main rupture zone occur in the high resistive zone (Oshiman et al., 2002; Tank et al., 2003). These electromagnetic surveys indicate that a resistive zone along an active fault is possibly related to an asperity along the fault with ordinary low-seismicity and episodic large earthquakes. Therefore, we claim that resistivity structures around active faults can be a good index for evaluation on fault activities and causes of seismic gaps. Although detailed seismicity mapping and GPS measurements can allow us to discuss asperities along a fault, they need long-term (more than

several years) and dense observations. Magnetotelluric surveys as introduced in this study can be done within several weeks, so that electromagnetic study is useful for a first evaluation of an asperity along active faults.

### 6.3. Lower crust conductors

Conductive zones in the lower crust are found below a depth of 12 km (C2 and C4 in Fig. 8). Kariya and Shankland (1983) indicate that the dry lower crust cannot explain the anomalously low resistivity because of low temperature. Seismic reflection surveys help us to discuss a possible cause of the low resistivity. Ito et al. (1993) and Ueno et al. (2002) found reflective layers in the Atotsugawa region at depth of 15–20 and 12–14 km, respectively. Conductive minerals in the lower crust cannot explain these reflectors, so that a possible candidate of the conductive lower crust is fluid. In addition, a depth at temperature of 400 °C in the Atotsugawa region is roughly estimated as 13.5 km by heat flow data (Uyeda and Horai, 1964). Jones (1987) proposed that an impermeable layer is created on the lower crust under a temperature of 400 °C, which keeps a conductive lower crust. Therefore, trapped fluid below an impermeable layer at the depth of about 12–15 km is a possible cause of the conductive lower crust around the Atotsugawa region.

A regional resistivity structure helps us to discuss the possible origin of fluid in the lower crust below the Atotsugawa Fault. Utada et al. (1996) investigated a large-scale resistivity structure below central Japan, and found a conductive lower crust and a thin conductive layer at the top of the subducting Philippine Sea Plate. They also found that the lower crustal conductor have contact with the slabtop conductor, and suggest that the supply of free water from the subducting Philippine Sea Plate is likely to be a source for the lower crustal fluid. Fluid content in the lower crust is roughly estimated by conventional Archie's law (Archie, 1942), often used to convert resistivity to porosity in systems where electrical conduction is dominated by an interconnected pore fluid. The Archie's law is written as

$$\rho_r = \rho_f \varphi^{-m}$$

where  $\rho_r$  is the effective resistivity of the rock,  $\varphi$  the porosity and  $m$  is a constant that lies between 1 and

2. If  $\rho_f$  is 1–0.1  $\Omega\text{m}$  at 400 °C after Nesbitt (1993), a porosity range of 0.03–5.8% is required to obtain resistivity of 300  $\Omega\text{m}$  in the conductive zone (C4). Similarly, a porosity range of 0.02–4.1% is required to obtain resistivity of 600  $\Omega\text{m}$  in the conductive zone (C2). These porosity values would be upper limits if solid-phase conductors, such as graphite (summarized in Wannamaker, 2000), had a contribution to conduction mechanism in the lower crust.

The lower crust is conductive below the low-seismicity area along the CAF (C4), while it is less conductive below the high-seismicity area (C2). We have no reasonable explanation for such heterogeneity of the lower crust conductor. One possible candidate may come from a different diffusion process of fluid from the lower crust to the surface. Below the WAF, fluid in the lower crust may upwell through the fracture zone along the WAF. The fluid concentration along the shallow part of the WAF (C1), higher than along the CAF (C3), can be explained by such upwelling fluid with high pore pressure. The released fluid is also consistent with many micro-earthquakes along the WAF (Fig. 2) because high pore pressure increased by fluid from a deep interior can result in micro-earthquakes (Sibson et al., 1988). On the other hand, fluid in the lower crust below the CAF, the possibly locked segment, may be preserved below a high resistive and possibly impermeable layer (R2) and result in the conductive layer (C4). Similar structures below large earthquakes have been reported by seismic and electromagnetic studies. Zhao et al. (1996) found a low velocity zone below the hypocenter of the 1995 Kobe earthquake (M7.2). They concluded that fluid-filled fractured rock matrix underlies the large earthquake zone, and is possibly related to the rupture nucleation of the earthquake. Gupta et al. (1996) found that the focal zone of the 1993 Latur earthquake ( $M_w$  6.1) was underlain by a low-velocity and low resistivity layer interpreted as a fluid-filled fractured rock matrix. Mitsuhashi et al. (2001) also found a deep conductive zone below the seismogenic region of the 1962 Northern Miyagi Earthquake (M6.5). These studies suggest that resistivity of the lower crust below an active fault can be also used as an index to evaluate fault and seismic activities. In order to confirm this hypothesis, a comparison between the seismicity and a spatial distribution of the lower crust conductor by a number of additional magnetotelluric surveys in the Atotsugawa region is necessary.

## 7. Conclusion

Magnetotelluric soundings were carried out across the Atotsugawa Fault. Two profiles were selected to be across the low-seismicity segment of the fault (CAF) and the high-seismicity segment (WAF). Although the spatial distribution of the strike direction shows the three-dimensionality in a shallow depth in the crust, two-dimensional resistivity structure was investigated by using the TM-mode of MT responses. The static-shift was corrected in the inversion procedure. The resistivity models along the two profiles are summarized as follows:

- (1) A lateral variation of resistivity structure is found below the WAF, with a northern highly and southern moderately resistive zones in the upper crust.
- (2) A highly resistive layer widely underlies the surface trace of the CAF.
- (3) A shallow low resistivity zone is recognized along the fault. The bottom of the low resistivity zone along the WAF is deeper than one along the CAF.
- (4) The lower crust of the Atotsugawa region is conductive. The resistivity in the lower crust below the WAF is higher than below the CAF.

A low resistivity zone along the fault is inferred as a fracture zone. Therefore, we conclude that the difference between the low resistivity zones along the WAF and the CAF reflects difference on fluid content or connectivity in the fracture zone. In addition, the lateral resistivity variation in the upper crust below the WAF indicates a sharp material boundary, while there is no corresponding lateral variation below the surface trace of the CAF. Both the shallow structure near the fault and the upper crustal structure support that the CAF is interpreted not as a creep segment, but possibly as a locked one. Thus, MT surveys around active faults give us useful information on fault activities, seismicity and seismic gaps along faults.

The conductive lower crust is also inferred to be due to fluid. The heterogeneity of the lower crustal resistivity is enigmatic, but may reflect a different diffusion process of fluid from the lower crust to the surface. It is suggested that the conductive lower crust beneath the CAF is recognized where fluid is trapped by an impermeable layer in the upper crust. On the other hand, fluid in the lower crust below the WAF may diffuse to the

surface through the fracture zone along the fault. Such upwelling fluid from the lower crust is consistent with many micro-earthquakes along the WAF.

## Acknowledgments

The authors thank Dr. K. Ito and H. Wada of Disaster Prevention Research Institute, Kyoto University for providing us hypocenter data around the Atotsugawa region and helpful discussion. Dr. H. Negishi, National Research Institute for Earth Science and Disaster Prevention, Japan, and Y. Shimada, RIKEN, Japan kindly gave us seismic velocity structures around the Atotsugawa region. We also thank Dr. S. Yamaguchi of Kobe University and Dr. I. Shiozaki of Tottori University for valuable comments and field assists. We thank Dr. T. Uchida and Dr. Y. Ogawa of Geological Survey of Japan for providing their inversion code of MT data. We are grateful to Dr. S. Sakanaka, Dr. M. Ichiki, Y. Hori, F. Hori, Dr. T. Kasaya, K. Tanimoto, Dr. M. Amita, and Y. Kobayashi for their assists on the fieldwork and useful discussion. Several figures are made using GMT produced by [Wessel and Smith \(1998\)](#). Two anonymous reviewers greatly improved the manuscript.

## References

- Amelung, F., King, G., 1997. Earthquake scaling laws for creeping and non-creeping faults. *Geophys. Res. Lett.* 24, 507–510.
- Archie, G.E., 1942. The electrical resistivity log as an aid in determining some reservoir characteristics. *Trans. Am. Inst. Min. Metall. Pet. Eng.* 146, 54–62.
- Chakridi, R., Chouteau, M., Mareschal, M., 1992. A simple technique for analyzing and partly removing galvanic distortion from the magnetotelluric impedance tensor: application to Abitibi and Kapuskasing data (Canada). *Geophys. J. Int.* 108, 917–929.
- Chiarabba, C., Amato, A., 1997. Upper crustal structure of the Benevento area (southern Italy): fault heterogeneities and potential for large earthquakes. *Geophys. J. Int.* 130, 229–239.
- deGroot-Hedlin, C., Constable, S.C., 1990. Occam's inversion to generate smooth, two-dimensional models from magnetotelluric data. *Geophysics* 55, 1613–1624.
- deGroot-Hedlin, C., 1991. Removal of static shift in two dimensions by regularized inversion. *Geophysics* 56, 2102–2106.
- Eberhart-Phillips, D., Labson, V.F., Stanley, W.D., Michael, A.J., Rodrigues, B., 1990. Preliminary velocity and resistivity models of the Loma Prieta earthquake region. *Geophys. Res. Lett.* 17, 2035–2038.
- Electromagnetic Research Group for the Active Fault, 1982. Low electrical resistivity along an active fault, the Yamasaki Fault. *J. Geomag. Geoelectr.* 34, 103–127.
- Gamble, T.D., Goubau, W.M., Clarke, J., 1979. Magnetotellurics with a remote magnetic reference. *Geophysics* 44, 53–68.
- Geographical Survey Institute, Japan, 1997. Crustal deformation in the Chubu and the Hokuriku region, Japan. *Rep. Coord. Comm. Earthquake Predict.* 57, 520-L 524 (in Japanese).
- Geological Survey of Japan, 1989. 1:200,000 Geological Map, Takayama.
- Groom, R.W., Bailey, R.C., 1989. Decomposition of magnetotelluric impedance tensors in the presence of local three-dimensional galvanic distortion. *J. Geophys. Res.* 94, 1913–1925.
- Gupta, H.K., Sarma, S.V.S., Harinarayana, T., Virupakshi, G., 1996. Fluids below the hypocentral region of the Latur earthquake. *Geophys. Res. Lett.* 23, 1569–1572.
- Gutenberg, B., Richter, C.F., 1944. Frequency of earthquakes in California. *Bull. Seismol. Soc. Am.* 34, 185–188.
- Handa, S., Sumitomo, N., 1985. The geoelectric structure of the Yamasaki and the Hanaori faults. *J. Geomag. Geoelectr.* 37, 93–106.
- Hirahara, K., Ooi, Y., Ando, M., Hoso, Y., Wada, Y., Ohkura, T., 2003. Dense GPS array observations across the Atotsugawa Fault, central Japan. *Geophys. Res. Lett.* 30, 8012, doi:10.1029/2002GL015035.
- Hirose, F., Nakamura, A., Hasegawa, A., 2002. *b*-value variation associated with the rupture of asperities – spatial and temporal distribution of *b*-value east off NE Japan. *Zisin 2nd Ser.* 55, 249–260 (in Japanese with English abstract).
- Iidaka, T., Iwasaki, T., Takeda, T., Moriya, T., Kumakawa, I., Kurashimo, E., Kawamura, T., Yamasaki, F., Koike, K., Aoki, G., 2003. Configuration of subducting Philippine Sea Plate and crustal structure in the central Japan region. *Geophys. Res. Lett.* 30, 1219, doi:10.1029/2002GL016517.
- Ito, K., Wada, H., 1999. Observation of micro-earthquakes in the Atotsugawa Fault region, central Honshu, Japan – seismicity in the creeping section of the fault. In: Ogasawara, H., Yanagidani, T., Ando, M., Balkema, A.A. (Eds.), *Proceedings of the Joint Japan–Poland Symposium on Mining and Experimental Seismology*, pp. 229–243.
- Ito, K., Kawasaki, I., Hurumoto, M., Isobe, H., Nagai, T., 1993. Seismic survey in northern Chubu district, Japan: Toyama–Kamitakara line. *Ann. Disas. Prev. Res. Inst., Kyoto Univ.* 36, 325–328 (in Japanese with English abstract).
- Jones, A.G., 1987. MT and reflection: an essential combination. *Geophys. J. Roy. Ast. Soc.* 89, 7–18.
- Jones, A.G., 1992. In: Fountain, D.M., Arculus, R., Kay, R.W. (Eds.), *Electrical Conductivity of the Continental Lower Crust, in Continental Lower Crust, Developments in Geotectonics* 23. Elsevier, pp. 81–144.
- Jones, A.G., Kurtz, R.D., Boerner, D.E., Craven, J.A., McNeice, G.W., Gough, D.I., DeLaurier, J.M., Ellis, R.G., 1992. Electromagnetic constraints on strike-slip fault geometry – the Fraser River fault system. *Geology* 20, 561–564.
- Jones, A.G., Groom, R.G., 1993. Strike angle determination from the magnetotelluric impedance tensor in the presence of noise and local distortion: rotate at your peril. *Geophys. J. Inter.* 113, 524–534.
- Kariya, K.A., Shankland, T.J., 1983. Electrical conductivity of dry lower crustal rocks. *Geophysics* 48, 52–61.

- Kasaya, T., Oshiman, N., Sumitomo, N., Uyeshima, M., Iio, Y., Uehara, D., 2002. Resistivity structure around the hypocentral area of the 1984 Western Nagano Prefecture earthquake in central Japan. *Earth Planets Space* 54, 107–118.
- Lay, T., Kanamori, H., Ruff, L., 1982. The asperity model and the nature of large subduction zone earthquake occurrence. *Earthquake Pred. Res.* 1, 3–71.
- Mackie, R.L., Livelybrooks, D.W., Madden, T.R., Larsen, J.C., 1997. A magnetotelluric investigation of the San Andreas fault at Carrizo Plain, California. *Geophys. Res. Lett.* 24, 1847–1850.
- Matsuda, T., 1966. Strike-slip faulting along the Atotsugawa Fault. *Bull. Earthq. Res. Inst.* 44, 1179–1212 (in Japanese with English abstract).
- Mikumo, T., Wada, H., Koizumi, M., 1988. Seismotectonics of the Hida region, central Honshu, Japan. *Tectonophysics* 147, 95–119.
- Mitsuhata, Y., Ogawa, Y., Mishina, M., Kono, T., Yokokura, T., Uchida, T., 2001. Electromagnetic heterogeneity of the seismogenic region of 1962 M.6.5 Northern Miyagi Earthquake, north-eastern Japan. *Geophys. Res. Lett.* 28, 4371–4374.
- Murakami, H., Yamada, I., Kobayashi, U., 1984. Geomagnetic total force anomalies associated with active fault – observation of the geomagnetic total force around Atotsugawa Fault and Atera fault. *Zisin 2nd Ser.* 37, 397–405 (in Japanese with English abstract).
- Nagai, R., Kikuchi, M., Yamanaka, Y., 2001. Comparative study on the source processes of recurrent large earthquakes in Sanriku-oki region: the 1968 Tokachi-oki earthquake and the 1994 Sanriku-oki earthquake. *Zisin 2nd Ser.* 54, 267–280 (in Japanese with English abstract).
- Nesbitt, B.E., 1993. Electrical resistivities of crustal fluids. *J. Geophys. Res.* 98, 4301–4310.
- Ogawa, Y., 1992. Deep crustal resistivity structure revealed by wide-band magnetotellurics – Tohoku and Hokkaido region. Ph.D. Thesis. University of Tokyo, 320 pp.
- Ogawa, Y., Uchida, T., 1996. A two-dimensional magnetotelluric inversion assuming Gaussian static shift. *Geophys. J. Int.* 126, 69–76.
- Oshiman, N., Honkura, Y., Kuge, K., Sakai, H., 1987. Electric and magnetic anomalies at the Atotsugawa Fault and their implications of fault activity. *J. Geomag. Geoelectr.* 39, 143–158.
- Oshiman, N., Yoshimura, R., Kasaya, T., Honkura, Y., Matsushima, M., Bari, S., Celik, C., Tuncer, M.K., Isikara, A.M., 2002. Deep resistivity structure around the fault associated with the 1999 Kocaeli earthquake, Turkey. In: Fujinawa, Y., Yoshida, A. (Eds.), *Seismotectonics at the Convergent*. Terra Science Publishing Company, Tokyo, pp. 293–303.
- Research Group for Active Faults, 1991. *Active Faults in Japan: Sheet Maps and Inventories*. University of Tokyo Press, 363 pp. (in Japanese).
- Rybicki, K.R., Yamashita, T., 2002. On faulting in inhomogeneous media. *Geophys. Res. Lett.* 10.1029/2002GL014672.
- Sagiya, T., Miyazaki, S., Tada, T., 2000. Continuous GPS array and present-day crustal deformation of Japan. *Pure Appl. Geophys.* 157, 2303–2322.
- Sibson, R.H., Robert, F., Poulsen, H., 1988. High-angle reverse faults, fluid pressure cycling, and mesothermal gold-quartz deposits. *Geology* 16, 551–555.
- Sugisaki, R., Ido, M., Takeda, H., Isobe, Y., Hayashi, Y., Nakamura, N., Satake, H., Mizutani, Y., 1983. Origin of hydrogen and carbon dioxide in fault gases and its relation to fault activity. *J. Geol.* 91, 239–258.
- Tank, S.B., Honkura, Y., Ogawa, Y., Oshiman, N., Tuncer, M.K., Matsushima, M., Celik, C., Tolak, E., Isikara, A.M., 2003. Resistivity structure in the western part of the fault rupture zone associated with the 1999 Izmit earthquake and its seismogenic implication. *Earth. Planets and Space* 55, 437–442.
- Uchida, T., 1993. Smooth 2D inversion for magnetotelluric data based on statistical criterion ABIC. *J. Geomag. Geoelectr.* 45, 841–858.
- Uchida, T., Ogawa, Y., 1993. Development of FORTRAN code for two-dimensional magnetotelluric inversion with smoothness constraint. Open-File Report, *Geol. Surv. Japan*, vol. 205, 115 pp.
- Ueno, T., Ito, K., Wada, H., Yoshii, K., Matsubara, K., 2002. Seismic survey along the Atotsugawa Fault system in Central Japan: Part 2. *Ann. Disas. Prev. Res. Inst., Kyoto Univ.* 45B, 577–590 (in Japanese with English abstract).
- Unsworth, M.J., Malin, P.E., Egbert, G.D., Booker, J.R., 1997. Internal structure of the San Andreas Fault Zone at Parkfield, California. *Geology* 25, 359.
- Unsworth, M.J., Egbert, G.D., Booker, J.R., 1999. High resolution electromagnetic imaging of the San Andreas Fault in Central California. *J. Geophys. Res.* 104, 1131.
- Unsworth, M.J., Eisel, M., Egbert, G.D., Siripunavaporn, W., Bedrosian, P.A., 2000. Along-strike variations in the structure of the San Andreas Fault at Parkfield, California. *Geophys. Res. Lett.* 27, 3021.
- Utada, H., Hamano, Y., Segawa, J., et al., 1996. Conductivity anomaly around the Japanese Islands. In: Isezaki, N. (Ed.), *Geology and Geophysics of the Japan Sea (Japan-USSR Monograph Series)*. Terra Science Publishing Company, Japan, pp. 103–149.
- Uyeda, S., Horai, K., 1964. Terrestrial heat flow in Japan. *J. Geophys. Res.* 69, 2121–2141.
- Wannamaker, P.E., Hohmann, G.W., Ward, S.H., 1984. Magnetotelluric responses of three-dimensional bodies in layered earths. *Geophysics* 49, 1517–1533.
- Wannamaker, P.E., 2000. Comment on ‘The petrologic case for a dry lower crust’ by Bruse W.D. Yardley and John W. Valley. *J. Geophys. Res.* 105, 6057–6064.
- Wessel, P., Smith, W.H.F., 1998. New, improved version of Generic Mapping Tools released. *EOS Trans. Am. Geophys. U.* 79 (47), 579.
- Wight, D.E., Bostick, F.X., 1980. Cascade decimation – a technique for real time estimation of power spectra. In: *Proceedings of the IEEE International Conference on Acoustic, Speech Signal Processing*, pp. 626–629.
- Zhao, D., Kanamori, H., 1995. The 1994 Northridge earthquake: 3D crustal structure in the rupture zone and its relation to the aftershock locations and mechanisms. *Geophys. Res. Lett.* 22, 763–766.
- Zhao, D., Kanamori, H., Negishi, H., Wiens, D., 1996. Tomography of the source area of the 1995 Kobe earthquake: evidence for fluids at the hypocenter? *Science* 274, 1891–1894.